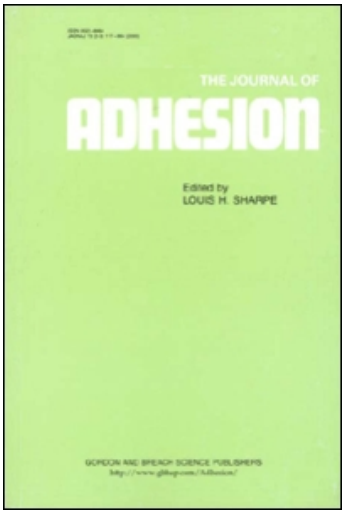

The Journal of Adhesion
Publication details, including instructions for authors and subscription information:
http://www.informaworld.com/smpp/title~content=t713453635

Localization of Phosphorylated Serine, Osteopontin, and Bone Sialoprotein on Bone Fracture Surfaces

P. J. Thurner[ab]; S. Lam[a]; J. C. Weaver[c]; D. E. Morse[c]; P. K. Hansma[b]
[a] School of Engineering Sciences, University of Southampton, Southampton, United Kingdom [b] Physics Department, University of California Santa Barbara, Santa Barbara, CA, USA [c] Department of Molecular, Cellular and Developmental Biology, University of California Santa Barbara, Santa Barbara, CA, USA

To cite this Article Thurner, P. J. , Lam, S. , Weaver, J. C. , Morse, D. E. and Hansma, P. K.(2009) 'Localization of Phosphorylated Serine, Osteopontin, and Bone Sialoprotein on Bone Fracture Surfaces', The Journal of Adhesion, 85: 8, 526 — 545
To link to this Article: DOI: 10.1080/00218460902996424
URL: http://dx.doi.org/10.1080/00218460902996424

The Journal of Adhesion, 85:526–545, 2009

ISSN: 0021-8464 print/1545-5823 online
DOI: 10.1080/00218460902996424

Taylor & Francis
Taylor & Francis Group

Localization of Phosphorylated Serine, Osteopontin, and Bone Sialoprotein on Bone Fracture Surfaces

P. J. Thurner[1,2], S. Lam[1], J. C. Weaver[3], D. E. Morse[3], and P. K. Hansma[2]

[1]School of Engineering Sciences, University of Southampton, Southampton, United Kingdom
[2]Physics Department, University of California Santa Barbara, Santa Barbara, CA, USA
[3]Department of Molecular, Cellular and Developmental Biology, University of California Santa Barbara, Santa Barbara, CA, USA

Bone mineral density or bone mass alone cannot reliably predict fracture risk in patients. It is generally accepted that bone quality, including the properties of the organic matrix of bone, should also be considered. Collagen type I accounts for about 90% of this organic matrix. The other 10% are accounted for by various proteins and proteoglycans usually summarized by the term noncollagenous proteins (NCPs). These NCPs have a large influence on the nanoscale organization of bone. In addition, some NCPs have intriguing properties that could strongly influence bone matrix material properties; they can form self-healing networks based on ion-mediated bonds. Such behavior was also reported for trabecular bone fracture surfaces, rejoined after cleavage. To obtain proof that this behavior of bone is due to NCPs, an immunohistochemical approach was chosen for the work presented in this communication. Antibodies for phosphoserine, which is abundant in many NCPs but not in collagen type I, as well as antibodies for osteopontin and bone sialoprotein, were used on human trabecular bone fracture surfaces and microfractured trabeculae. Signals were detected using secondary gold-labeled antibodies and backscattered scanning electron microscopy. We found homogenous NCP coverage of fracture surfaces and elevated signals on bridging ligaments. Osteopontin and bone sialoprotein were detected in localized patches. Overall, this work suggests that the self-healing effect of trabecluar bone fracture surfaces, rejoined after cleavage, can be explained by the presence of NCPs. In addition, we conclude that NCPs also constitute the interface that is disrupted when bone

Received 24 November 2008; in final form 18 March 2009.

One of a Collection of papers honoring J. Herbert Waite, the recipient in February 2009 of *The Adhesion Society Award for Excellence in Adhesion Science, Sponsored by 3M*.

Address correspondence to P. J. Thurner, Bioengineering Science Research Group, University of Southampton, Highfield, Southampton, SO17 1BJ, UK. E-mail: p.thurner@soton.ac.uk

fails, attributing them high importance for bone matrix material properties and fracture risk.

Keywords: Bone Sialoprotein; Immunhistochemistry; Microfracture; Noncollagenous Proteins; Osteopontin; Phosphoserine; Trabecular Bone

INTRODUCTION

The molecular origin of mechanical competence of bone is not fully understood. Bearing in mind that bone essentially is an organic-inorganic composite material with nanoscale building blocks, this is not all surprising. As there exists a magnitude of different components and as bone is structured hierarchically, it is a challenging task to separate principal atomistic effects that are influencing the apparent mechanical properties of bone. Traditionally, it has been the inorganic hydroxyapatite phase that was hypothesized to be the most important factor influencing the mechanical properties of bone, as it supplies stiffness and structure. In fact, the mineral phase, or rather the amount of mineral a patient has, is, to date, essentially the most commonly and only diagnostic surrogate used to assay fracture risk. That this strategy is not able to accurately diagnose all people that actually exhibit a high fracture risk is evident from medical case studies [1]. Hence, the interest to understand bone as a composite material, taking into account the organic portion of bone, is growing. This organic portion consists mainly of collagen type I in the form of fibrils with typical diameters of 80–100 nm and lengths of up to 10 μm or more [2]. A smaller part of it (∼10%) consists of other proteins and proteoglycans, which are usually summarized by the term non-collagenous proteins (NCPs) [3]. Whereas collagen type I fibrils are the major protein providing a scaffold for mineralization, the NCPs are essentially the nanoscale engineers organizing tissue nanostructure and joining organic and inorganic components together. They are responsible for crystal nucleation, crystal growth, shape, and orientation [4–7]. They also provide adhesion to collagen and the hydroxyapatite mineral crystals [7–9] and are, hence, involved in forming the basic building block of bone, the mineralized collagen fibril. On the lowest ultrastructural level, bone is composed of these mineralized collagen fibrils, arranged in a parallel fashion. When trabecular bone fails due to compressive or tensile mechanical overload, the main fracture mechanism at the ultrastructural level seems to be the delamination of these fibrils, as was concluded from scanning electron as well as atomic force microscopy studies of bone

fracture surfaces [10,11]. Micrographs obtained from both techniques showed that fracture surfaces of healthy bone usually exhibit collagen fibrils with their intact coating of hydroxyapatite crystals. Force spectroscopy studies of such surfaces showed an intriguing effect; remarrying two fractured surfaces by pressing them together re-established some bonds such that they resisted their subsequent separation [12]. Importantly, energy dissipation was repeatable and significantly higher in the presence of Ca^{2+} ions. This effect had already been reported from previous force spectroscopy studies on polished bone surfaces [13], but only more recent work could link the effect found to NCPs as similar mechanical signatures were also found in network of purified proteins [14]. Where hints of an unstructured adhesive component in bone had been detected in earlier work, the composition of this adhesive had not been analyzed but the findings mentioned above led us to the hypothesis that the adhesive or glue consists of NCPs. A material model based on this hypothesis has previously been proposed [15,16]. Adding even more to the importance of NCPs, this hypothesis is also the basis for the work presented in this communication. In order to assess bone fracture and the involvement of adhesive and cohesive interfaces made from NCPs, we used immunohistochemistry to label freshly fractured bone surfaces, as well as microfractures, within larger trabecular bone samples for NCPs in a generic fashion by targeting phosphoserine, as well as by using specific antibodies targeting osteopontin (OPN) and bone sialoprotein (BSP).

MATERIALS AND METHODS

Sample Preparation

We investigated bone samples isolated from lumbar vertebrae of a previously healthy male donor 24 years of age with no diagnosed bone disease. The human vertebrae were acquired through the National Disease Research Interchange (NDRI, Philadelphia PA, USA); handling of material and all experiments were conducted at the University of California Santa Barbara adhering to all local ethical standards. Two different types of samples were produced. For mechanical testing and subsequent immunohistochemical treatment, bone samples with a height of about 4 mm and a cross-sectional area of about 5×5 mm were cut from vertebrae using a bandsaw (Marmed, Inc., Cleveland, OH, USA) under constant irrigation with tap water. The smaller sample dimension was oriented in the original principal load-bearing direction. For immunohistochemical treatment only, strips of bone samples were made with the same bandsaw having a cross-sectional area of

about 1×1 mm and a length of 10 mm. Bone marrow was extracted from all specimens using a jet of pressurized water. Using two pairs of tweezers the smaller strips were fractured in their wet state into pieces of roughly cubiodal shape just prior to the immunohistochemical treatments.

Immunohistochemistry

Labeling for phosphoserine, OPN, and BSP was done as described below. All solutions containing buffers, as well as the buffers themselves, had a pH of 7.4. All incubations were performed at room temperature on a 2D shaker (G75, New Brunswick Scientific, Edison, NJ, USA). Monoclonal antibodies for human OPN (LFMB-14) [17] and human BSP (LFMB-25) [17] were a gift from Larry W. Fisher NIH/NICDR. A full protocol for the immunohistochemistry is given in the Appendix. In brief, samples were blocked in Tris-buffered saline (TBS) containing 1% bovine serum albumin and 0.05% Tween® (blocking buffer) and then incubated with primary antibody in blocking buffer at dilutions of 1:5, 1:50, and 1:500 (anti-phosphoserine) and 1:80, 1:800, and 1:8000 (anti-OPN, anti-BSP). After washes, and repeated blocking, samples were incubated with the secondary antibody in blocking buffer at a dilution of 1:50. Finally, samples were washed in tap water as well as HPLC grade water, exposed to silver enhancement, and dried for scanning electron microscopy (SEM).

Mechanical Testing

Compression testing of larger samples was done using a custom-made mechanical testing device described in detail in [10]. The sample chamber had a fluid inlet and outlet, alowing for immersion of the specimen in fluid, in this case TBS-Buffer, at pH 7.4 A strain rate of 50%/s was used for all mechanical tests. The mechanical tests consisted of two phases: in the first phase, the piston was lowered slowly until a preload of 0.5 N was reached, in order to find the sample top, in the second phase, the sample was then loaded at a constant strain rate up to 18% apparent strain. Stress strain curves were corrected for the toe regions they exhibited at low strains: a linear fit performed in the elastic region (*i.e.*, the most linear region) of the stress strain curve was extrapolated and its intersection with zero stress was defined as the true zero strain [18]. From these corrected stress strain curves, elastic modulus, yield stress and strain, as well as failure stress and strain were retrieved. Failure was defined as the first local maximum

TABLE 1 Mean (N = 5) Elastic Modulus, Yield Stress and Strain, as Well as Failure Stress and Strain of Human Vertebral Trabecular Bone Samples Tested in Compression. The Data are in Good Agreement with Previously Published Data Obtained from Trabecular Bone (35)

Parameter	Average	Standard deviation
Elastic modulus (MPa)	134	34
Yield stress (MPa)	5.77	0.91
Yield strain (%)	4.5	1.0
Failure stress (MPa)	6.8	1.0
Failure strain (%)	7.4	1.0

in each stress-strain curve. The average values of the extracted parameters for five of the larger samples are given in Table 1.

High-Speed Photography

We used an Ultima 512 high-speed camera (Photron Inc., San Diego, CA, USA) equipped with a KC lens, with a KC-AUX, and an IF-3 lens mounted on top (Infinity, Boulder, CO, USA). The high-speed camera can record up to 32,000 frames/s but offers limited memory of 512 MB. We recorded images at 500 frames/s and a shutter opening time of 1/10000 s. The scene was illuminated from the front using two fiber lights (MH-100, Dolan Jenner Industries, Inc., Lawrence, MA, USA) at angles of about $\pm 45^{\circ}$.

Image Processing

High-Speed Photography

All recorded movies where cropped to the region of the mechanical test using Image J (National Institutes of Health, Bethesda, MD, USA). A texture correlation [19] algorithm was then applied using LabView (National Instruments, Austin, TX, USA) on the individual frames in order to detect the motion of the plunger. A region of interest with high contrast was selected on the plunger and tracked in subsequent recorded frames. The tracking allowed synchronization between recorded image data and stress-strain curves. For the quantification of whitening seen during compression of the samples, a thresholding algorithm, programmed in LabView, was used as previously described in detail [10].

Scanning Electron Microscopy

The number of particles in the backscattered electron images was determined by an adaptive local thresholding and component labeling

[20] algorithm. 16 × 16 pixel interrogation windows were used for local thresholding.

The average gray value was computed for each interrogation window subsequently, the threshold was set to values from 1.1 to 2 (in steps of 0.1) times this average gray value. For each step, the number of particles was computed and plotted in a graph against the threshold value. The final threshold was computed from two linear fits of the initial (large negative) and final (small negative, close to zero) slope observed in this graph. The fitting boundaries were selected manually. Typical values for the threshold multiplication factor were between 1.3 and 1.4.

Scanning Electron Microscopy (SEM)

For electron microscopy the samples were rinsed briefly with HPLC grade water to remove residual buffer. The large samples from compression testing were then transferred to a custom-made aluminum vise, air-dried at 37°C overnight, contacted with silver paint, and carbon-coated. The small samples were carefully blotted dry on a Kim-wipe® and then thoroughly dried in a desiccator overnight. Subsequently, the samples were mounted on a small metal bar using silver-paint. The bar had a tapped hole in its center, so it could be mounted on a custom sample holder in a way that both fractured surfaces of each sample were accessible and carbon coated, as shown in Fig. 1. Imaging

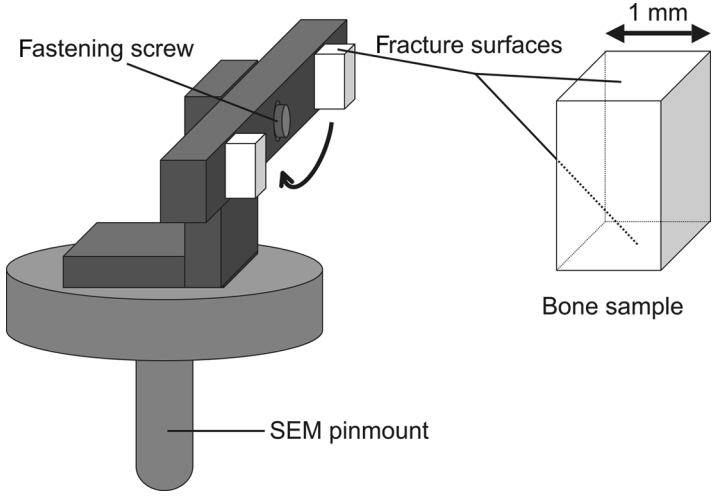

FIGURE 1 Schematic of the sample holder for SEM with two mounted samples. The bar can be rotated making both labeled fractured surfaces accessible.

was done with a Vega TS 5130MM SEM (Tescan, Brno, Czech Republic) in secondary and backscattered imaging mode at an accelerating voltage of 20 kV. In addition, a few high-resolution SEM images (magnification 10 k–100 k) were acquired using a XL30 Sirion FEG SEM (FEI Company, Hillsboro, OR, USA) in secondary and backscattered imaging mode at accelerating voltages between 5 and 15 kV.

RESULTS

An overview of the typical fracture surfaces observed in the small samples is presented in Fig. 2. The different morphologies can be

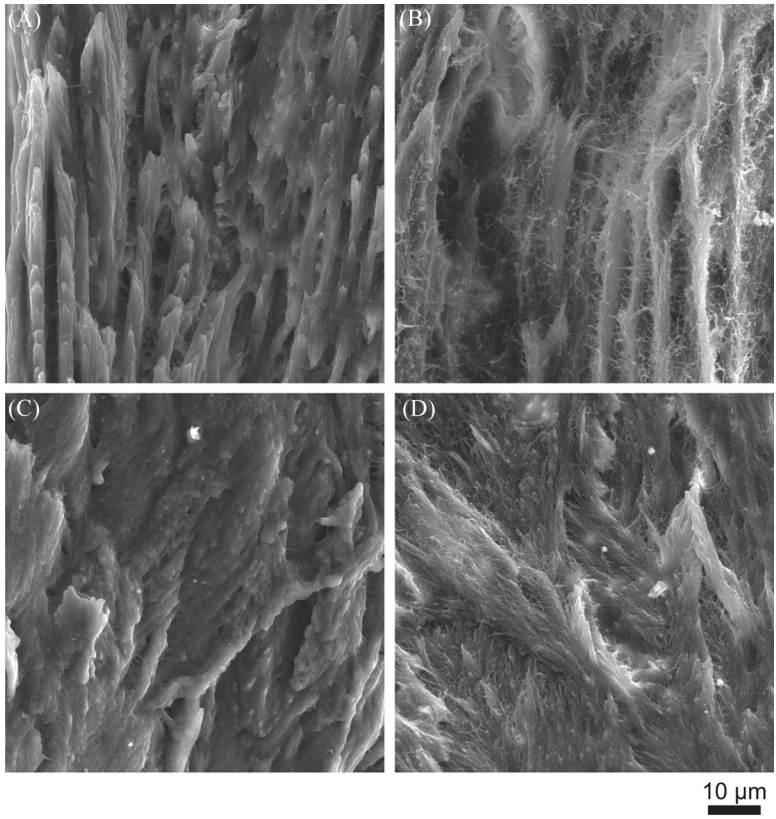

FIGURE 2 Overview of fracture surface morphologies observed with SEM on small (1 mm^3) trabecular bone samples. The morphologies arise from orientation of the fracture surface perpendicular (A and B) or parallel (C and D) to bone lamellae. In addition, different amounts of small fibers are observed (A and C *vs*. B and D).

explained by different fracture orientations. Trabecular bone is arranged in a lamellar fashion; hence, orientation of the fracture surface perpendicular (Fig. 2A and B) or parallel (Fig. 2C and D) to the lamellae produces either rough or smooth surfaces, respectively. In addition, we also observed different levels of small fibers (fiber pull-out) in these SEM images; however, the origin of these differences was not clear. We did not observe an influence of surface morphology on labeling intensity. As can be seen from Fig. 3, we detected a high concentration of phosphoserine in fractured bone surfaces and statistical analysis of counted particles showed that the differences between labeled samples and negative controls were significant (Fig. 4). Higher resolution SEM investigations showed that phosphoserine, generally exposed on fracture surfaces, was also present on small bridging ligaments (Fig. 5), which have been reported to provide bone with increase fracture toughness [21]. In order to study bone failure in a more realistic setting, we loaded larger trabecular bone samples in compression to create microfractures, as shown in Fig. 6. Using high-speed photography and the previously reported stress-whitening effect in bone, we were able to optically detect microdamage and microfracture (Fig. 7), and

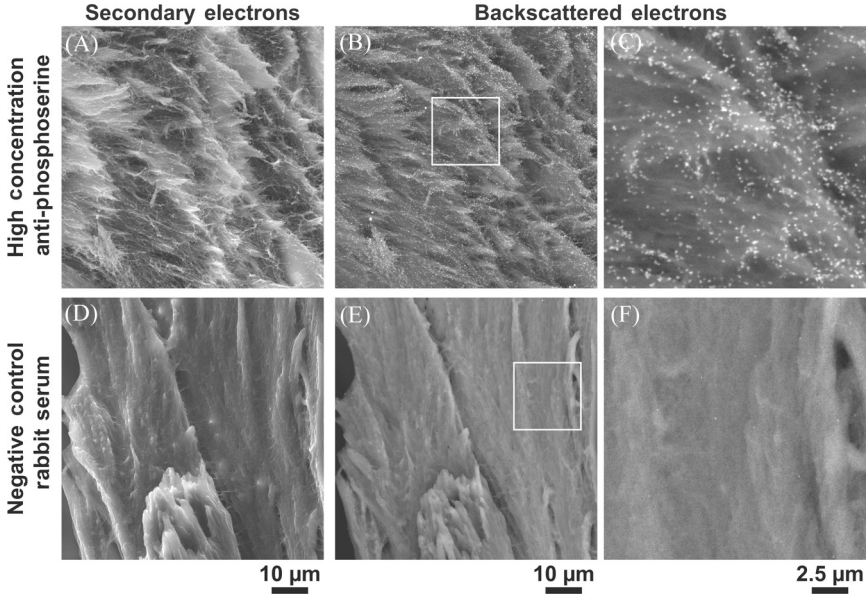

FIGURE 3 SEM image of fracture surfaces labeled for phosphoserine and negative control in secondary and backscattered electron imaging mode. Phosphoserine is detected homogenously across the surface.

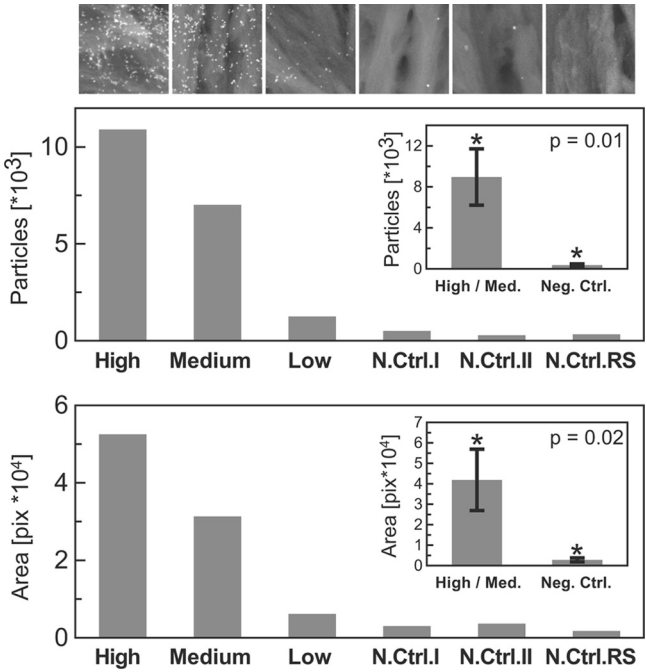

FIGURE 4 Results from particle detection algorithm analysis show a linear behavior of detected particles and labeled area in relation to concentration of the primary antibody. Detected particles and area from high (1:5) and medium (1:50) concentrations are significantly higher than values detected for the negative controls.

using SEM, we observed intense labeling signals on fractured surfaces as well as on a bridging ligament. Labeling of smaller samples for OPN and BSP did not give reliable signals in all experiments, which could be due to the fact that the epitope targeted for labeling is not exposed in all locations. Nevertheless, significant signals for OPN and BSP were detected (as can be seen in Figs. 8 and 9) within features that look like patches of NCPs and similar to the previously reported putative adhesive phase [12,22].

DISCUSSION

The role of NCPs in bone structure and function is still a vast area of research. Although there exist numerous excellent *in vivo* and *in vitro* studies on NCPs, conclusive evidence of the distinct roles and functions of NCPs in a materials science context, *i.e.*, the relationship

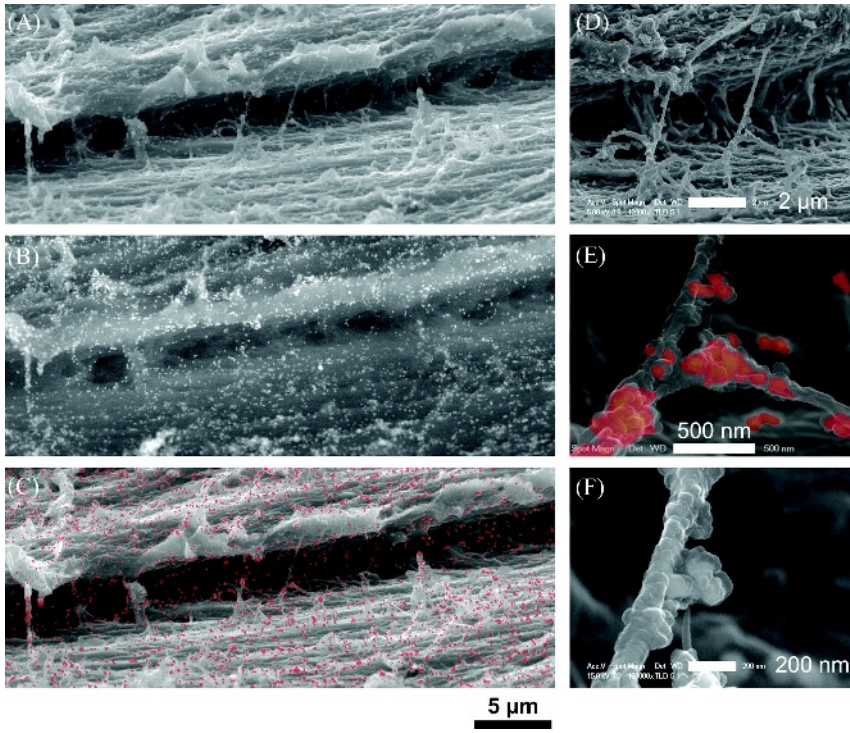

FIGURE 5 SEM images of a fractured surface at higher magnifications obtained in secondary (A, D, F) and backscattered (B) electron imaging mode. Particles detected in backscattered mode are also shown as colored overlays (C and E), which show that phosphoserine is also detected on bridging ligaments.

between ultrastructural organization and mechanical function, is limited. This is not surprising as bone is a very complex hierarchical composite material and both major organic and inorganic structural components, *i.e.*, collagen type I fibrils and carbonated hydroxyapatite crystals, are small with typical sizes between 1 nm and 500 nm (except for collagen fibril length). Therefore, investigations of the NCPs, influence on crystal growth or fibril assembly are rare. However, understanding of the processes involved in mineralization and maturation of bone tissue and associated changes due to age and disease have the potential for new diagnostics and therapies for patients with high fracture risk. Whereas the role of collagen for the mechanical function of bone and the effect of changes in covalent crosslinking of collagen is perhaps better understood [23], the concept of crosslinking, both

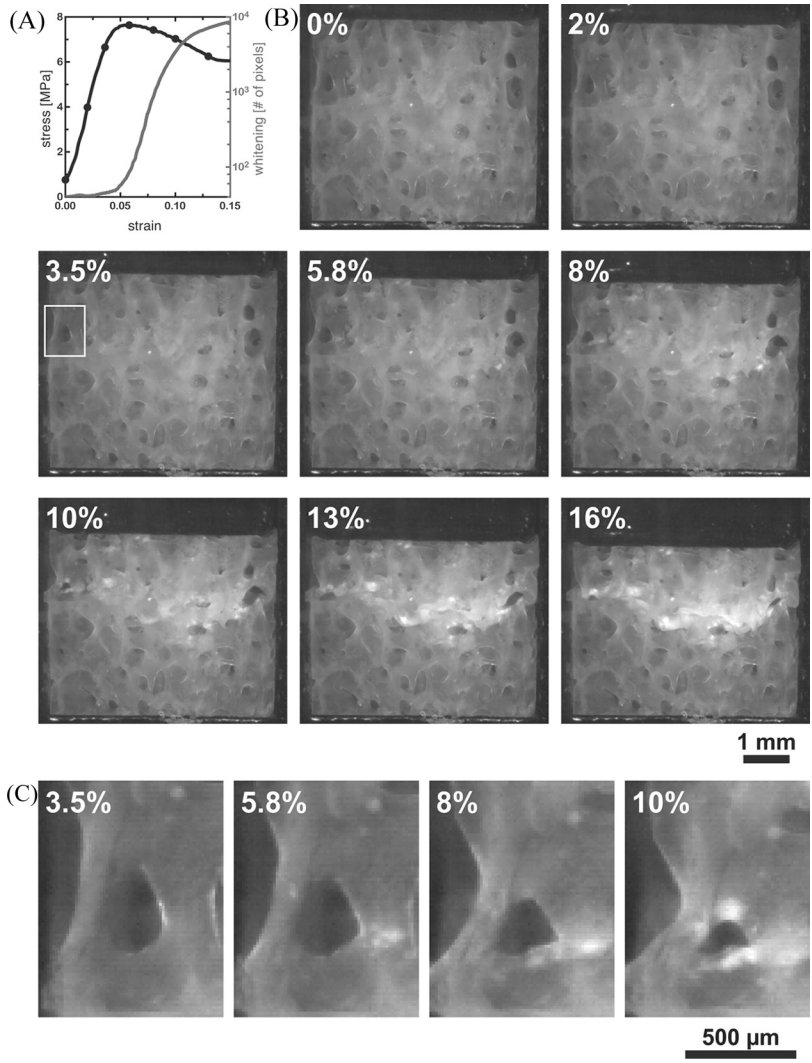

FIGURE 6 (A) Stress-strain and whitening–strain curve of a larger trabecular bone sample ($4 \times 4 \times 5\,mm^3$) as well as (C) corresponding photographic images of the sample during compression and a region of interest (indicated with a white frame in B), showing a microfracture occurring during compression.

covalent and through salt-bridges, of NCPs in the bone matrix and a possible mechanical function based on this phenomenon are relatively new. It has been shown that OPN and other NCPs are located

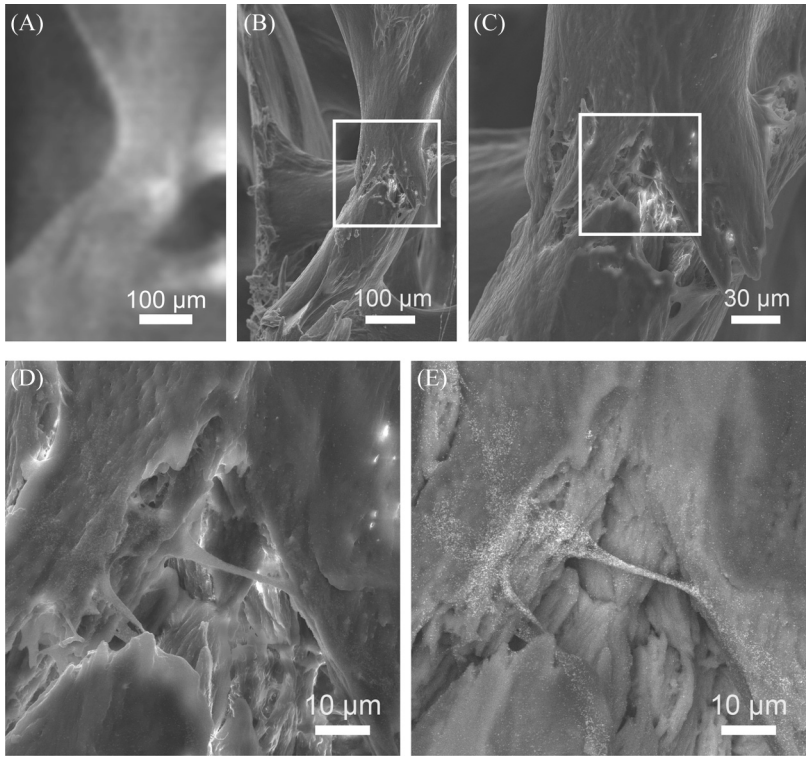

FIGURE 7 Comparison of (A) photographic and (B–E) SEM images of the microfractured trabecula. At higher magnification, a bridging ligament can be seen and the backscattered image (E) reveals intense labeling signal for phosphoserine on this ligament.

throughout the bone matrix in the interfibrillar space and are enriched in some areas such as cement lines [24].

Hence, given an abundance of proteins, there is room for speculation that these proteins could indeed have a significant influence on the mechanical properties of bone. It has been shown that some of the NCPs, among them OPN, have the ability to form homotypic and heterotypic covalent crosslinks when being exposed to the Transglutaminase enzyme [7,25], creating large polymeric structures. Using immunohistochemistry, such crosslinks have been detected in the periosteum and lacunae, but so far not in the bulk of bone [7]. In addition to covalent crosslinking, NCPs such as OPN, BSP, or DMP-1, with abundant negative charges, are also able to form networks based on relatively weak bonds mediated through ions with more than one

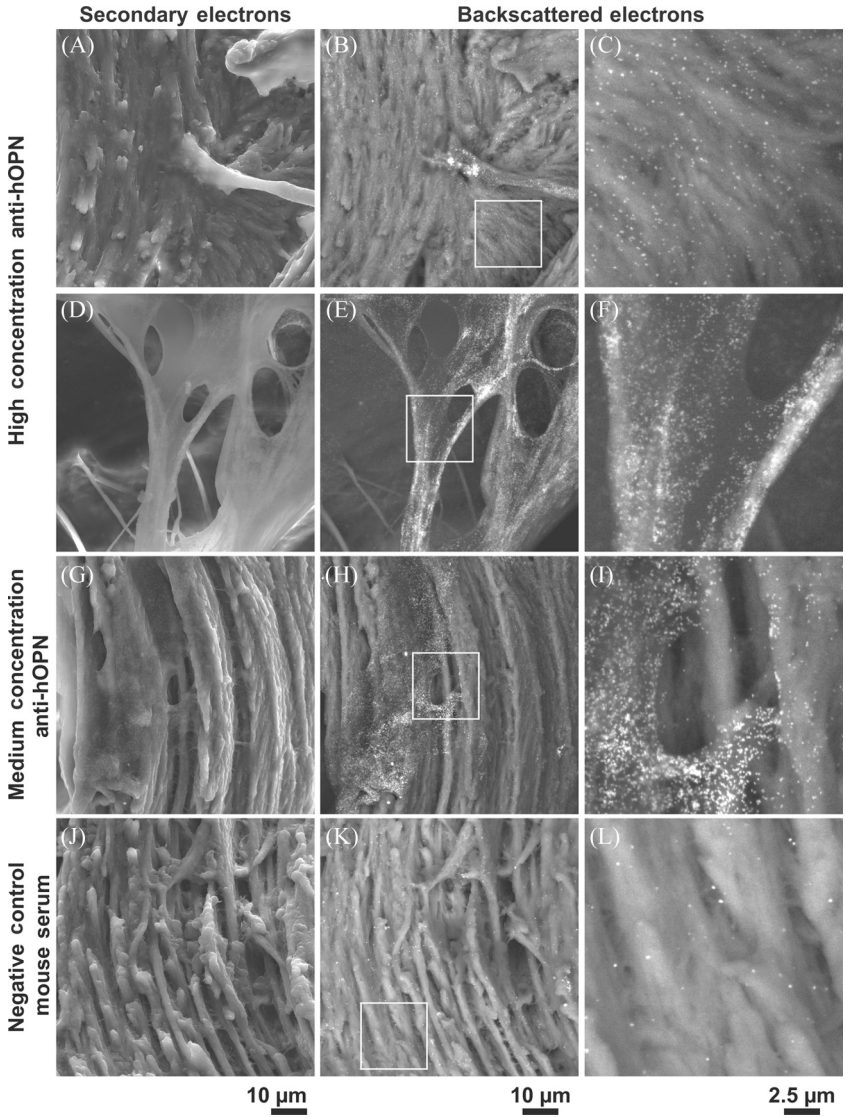

FIGURE 8 Secondary and backscattered electron images of fractured surfaces of small samples labeled for (A–I) OPN and (J–L) comparison to a negative control. Elevated signals for OPN are detected in patches.

positive charge [14,26]. These salt-bridges, also called sacrificial bonds, are easily broken when a protein network is loaded in a tensile fashion. Breaking of such a bond can expose a further portion

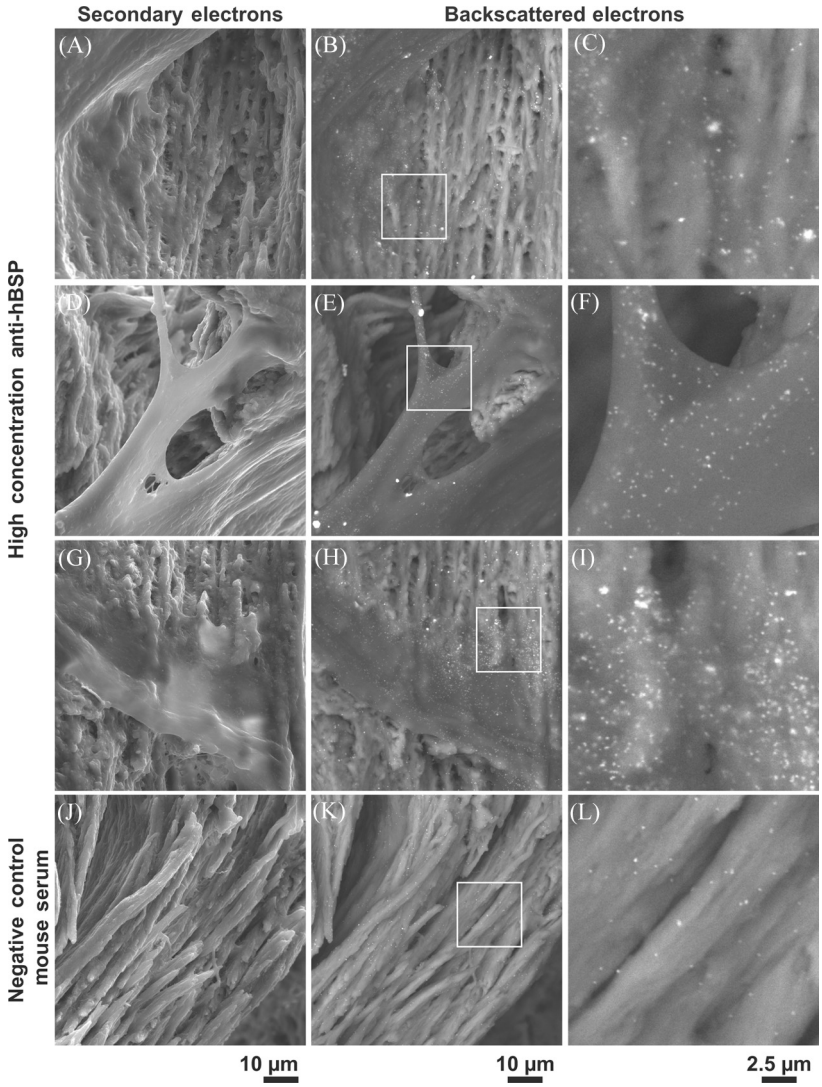

FIGURE 9 Secondary and backscattered electron images of fractured surfaces of small samples labeled for (A–I) BSP and (J–L) comparison to a negative control. Similar as for OPN, elevated signals for BSP are also detected in patches.

(hidden-length) of the network to the applied stress and increase the toughness of the network. The key aspect of the resulting sacrificial-bond-hidden-length mechanism is that upon relaxation,

the weak bonds can reform and, hence, similar amounts of energy can be repeatedly dissipated [13,14]. From experiments using atomic force microscopy in force spectroscopy mode, it was found that networks of OPN, BSP, and DMP-1 offer both high adhesion and cohesion [14,26]. An investigation of similar networks using the surface force apparatus confirmed high cohesion of OPN networks, but showed also that these networks were not necessarily good adhesives for any given substrate [27] and, similar to mussel foot protein (MFP), forming attachment plaques might require shear forces for activation [28]. In this light, the ability of NCPs to bind to collagen and the mineral crystals might also be critical for mechanical competence.

The most important result of this study is that fracture surfaces of healthy human trabecular bone are densely covered with NCPs. This corroborates the hypothesis that they form an interface between the mineralized collagen fibrils, and that it is this interface that is being disrupted when bone fails. Hence, any beneficial adhesive or cohesive mechanical properties of these proteins or networks, either covalent or through salt-bridges formed by them, would be effective in this interface. The properties of the interface would contribute more towards the mechanical properties if loads were acting perpendicular to the long axis of the collagen fibrils. But even in the case of a load acting parallel to the long axis of the collagen fibrils, there are scenarios in which this interface can be crucially important, namely in the case of fibrils sliding along each other as proposed by Gupta and Ziopous [29]. In addition, it has been shown in cortical bone that cracks, once initiated, usually follow a direction parallel to the long axis of collagen fibrils [21,30,31]. Also, in this case the properties of the interfibrillar interface should significantly influence the ease of crack propagation, *i.e.*, fracture toughness.

Although the amount of protein in terms of weight or volume is small, it is large on a molar scale. A basic estimation based on the energy dissipation measured in force spectroscopy experiments shows that only a few percent (in weight) would be sufficient to explain the strength of cortical bone [12]. Hence, it would be beneficial to quantify the amount of protein on such fracture surfaces. Although the quantitative image analysis presented here allows us to count the number of detected particles, it is difficult from this study to estimate how much protein actually is present on these surfaces. This is due to the fact that, due to blocking, the concentration of primary and secondary antibodies, as well as the size of the antibody complexes and morphology, not all epitopes can actually be reached. Hence, the quantitative numbers provide at best a lower limit for the protein density. Therefore, the area density of about 2.2 proteins/μm^2, based on particle

counting, is much lower than the protein area densities of 5×10^5 proteins/μm^2, as previously predicted [12]. The number of particles could be used to estimate the amount of protein present on the surface; however, we have no control of blocking of labeling sites by the blocking agent used as well as steric hindrance imposed by primary and secondary antibodies, *i.e.*, binding to labeling sites, and through this inhibit other antibodies to bind to neighboring sites and proteins due to their size. Also, we do not see the number of particles plateau at the three different concentrations used, which would be reached when all accessible epitopes have antibodies bound to them. This could be changed by usage of higher concentrations, greater volumes, and longer labeling times but, even then, there would still be a number of unknown parameters. However, the particle counting algorithm allows us to make a quantitative statement regarding the specificity of our labeling approach, as shown in Figs. 4 and 10; using Students' t-test, statistical comparison of detected particle numbers from samples labeled with high and medium concen-

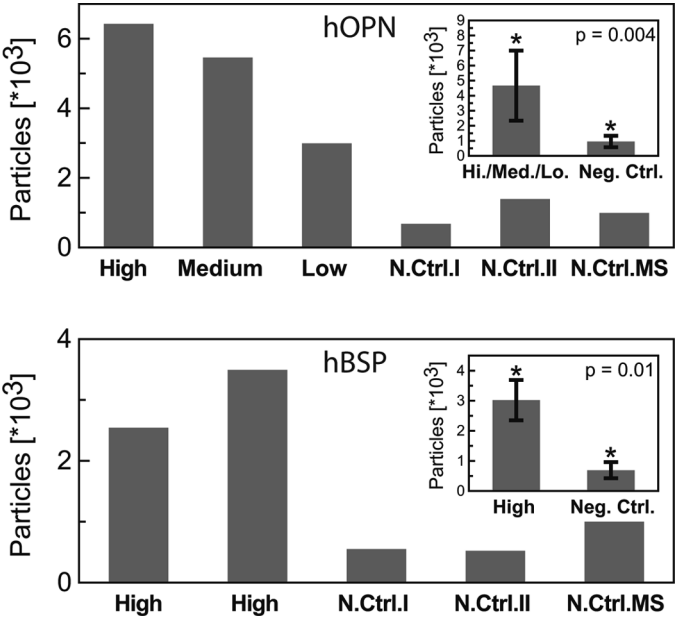

FIGURE 10 Particles detected in SEM image of samples labeled for OPN and BSP. Comparison of labeled samples with negative controls show that the number of particles detected in both cases is significantly higher compared to the negative controls.

trations of the primary antibodies were, in all cases, significantly different from numbers observed in the negative controls. The fact that both OPN and BSP (see Figs. 8 and 9) do not give homogenous signals, but are rather detected in irregular patches, is consistent with previous reports [32–34]. Applying the labeling protocol for phosphoserine, we also investigated the exposure of NCPs in a more realistic setting. Video footage of a larger specimen tested in compression to apparent strains of 16% is shown in Fig. 6. The high-speed photographs acquired during the experiment allow detection of deformed trabeculae *via* the whitening effect and gave us the opportunity to look inside a microfracture, where we detected a high concentration of phosphoserine on a bridging Fig. 10 ligament as shown in Fig. 7.

CONCLUSIONS

In summary, these results present proof that NCPs in bone are located on surfaces created during fracture. This suggests that the self-healing effect of re-married bone fracture surfaces can be explained by the presence of NCPs. And, from this, we can conclude that NCPs also constitute, at least in part, the interface that is disrupted when bone fails, suggesting a high importance of NCPs for bone matrix material properties and fracture risk.

ACKNOWLEDGMENTS

The authors would like to thank J. Herbert Waite and Emin Oroudjev for insightful discussions. For funding of this work we are gratefully indebted to NIH grant RO1 GM65354.

APPENDIX–PROTOCOLS FOR IMMUNOHISTOCHEMISTRY

Labeling for phosphoserine:

1. Blocking in 1.5 mL Tris-buffered saline (TBS), 1% bovine serum albumin (BSA) (Product Number A3059, Sigma-Aldrich, St. Louis, MO, USA), 0.05% Tween 20® (Product Number P9416, Sigma-Aldrich) for 1 h;
2. Labeling in 200 μL (500 μL) anti-phosphoserine from rabbit (Product Number AB1603, Chemicon International Inc., Temecula, CA, USA) in TBS, 1% BSA, 0.05% Tween 20® (concentrations of 1:5, 1:50, and 1:500) for 3 h;
3. Washing in 2 mL TBS, 0.05% Tween 20, 5 times for 5 min each;

4. Blocking in 1.5 mL TBS, 1% BSA, 0.05% Tween 20, 1% normal goat serum (Product Number G9023, Sigma-Aldrich) for 1 h;
5. Labeling in 200 μL (500 μL) secondary antibody—goat anti-rabbit with 20 nm Au colloids (Product Number EM.GAR20, BBInternational, Ltd., Cardiff, UK)—in TBS, 1% BSA, 1% goat serum, 0.05% Tween 20 (concentration of 1:50) for 3 h;
6. Washing in 2 mL TBS, 0.05% Tween 20, 3 times for 10 min each;
7. Washing in 2 mL de-ionized water, 3 times for 5 min each and in 2 mL HPLC-grade water (Product Number 270733, Sigma-Aldrich), 3 times for 5 min each;
8. Incubate with 200 μL (500 μL) silver enhancement for 18 min;
9. Washing with 2 mL tap water for 10 min and 2 mL HPLC-grade water for 10 min and 5 min;
10. Dried overnight in a desiccator.

Labeling for OPN and BSP

1. Blocking in 1.5 mL TBS, 1% BSA, 0.05% Tween 20 for 1 h;
2. Labeling in 200 μL anti-hOPN (LFMB-14 from mouse, [17]) or anti-hBSP (LFMB-25 from mouse, [17]) in TBS, 1% BSA, 0.05% Tween 20 (concentrations of 1:80, 1:800, and 1:8000) for 1 h;
3. Washing in 2 mL TBS, 1% BSA, 0.05% Tween 20, 9 times for 5 min each;
4. Blocking in 1.5 mL TBS, 1% BSA, 0.05% Tween 20, 1% normal goat serum for 1 h;
5. Labeling in 200 μL secondary antibody—goat anti-mouse with 20 nm Au colloids (Product Number EM.GMHL20, BBInternational Ltd., Cardiff, UK)—in TBS, 1% BSA, 1% goat serum, 0.05% Tween 20 (concentration of 1:50) for 1 h;
6. Washing in 2 mL TBS, 1% BSA, 0.05% Tween 20, 3 times for 10 min each;
7. Washing in 2 mL de-ionized water, 3 times for 5 min each and in 2 mL HPLC-grade water, 3 times for 5 min each;
8. Incubate with 200 μL silver enhancement for 18 min;
9. Washing with 2 mL tap water for 10 min and 2 mL HPLC-grade water two times for 10 min each;
10. Dried overnight in desiccator.

Negative controls: For each experiment, three negative controls were done, since the labeling procedure consisted in all cases of two antibodies and silver enhancement of the Au colloids attached to the secondary antibody. Therefore the negative controls consisted of:

1. Applying blocking buffer instead of the two antibodies (Steps 2 and 5) and subjecting the samples to silver enhancement (NC I);
2. Applying blocking buffer instead of the primary antibody (Step 2) and subjecting the samples to the secondary antibody and the gold enhancement (NC II);
3. Applying the same concentration of normal serum of the animal where the primary antibody was raised *i.e.*, rabbit (Product Number R9133, Sigma-Aldrich) or mouse (Product Number M5905, Sigma-Aldrich), instead of the primary antibody (Step 2) and subjecting the samples to the secondary antibody and the gold enhancement (NC RS, *i.e.*, rabbit serum or NC MS, *i.e.*, mouse serum).

REFERENCES

[1] Wainwright, S. A., Marshall, L. M., Ensrud, K. E., Cauley, J. A., Black, D. M., Hillier, T. A., Hochberg, M. C., Vogt, M. T., and Orwoll, E. S., *J. Clin. Endocrinol. Metab* **90**, 2787–2793 (2005).
[2] Weiner, S. and Wagner, H. D., *Annu. Rev. Mater. Sci.* **28**, 271–298 (1998).
[3] Grynpas, M. D., Tupy, J. H., and Sodek, J., *Bone* **15**, 505–513 (1994).
[4] Hunter, G. K. and Goldberg, H. A., *Proc. Natl. Acad. Sci. USA* **90**, 8562–8565 (1993).
[5] Hunter, G. K. and Goldberg, H. A., *Biochem. J.* **302 (Pt 1)**, 175–179 (1994).
[6] Qiu, S. R., Wierzbicki, A., Orme, C. A., Cody, A. M., Hoyer, J. R., Nancollas, G. H., Zepeda, S., and De Yoreo, J. J., *Proc. Natl. Acad. Sci. USA* **101**, 1811–1815 (2004).
[7] McKee, M. D. and Kaartinen, M. T., *Aging, Osteoporosis and Dental Implants* (Quintessence Pub. Co. Inc., Carol Stream, IL, 2002). Ch. 15, pp. 191–205.
[8] Tye, C. E., Hunter, G. K., and Goldberg, H. A., *J. Biol. Chem.* **280**, 13487–13492 (2005).
[9] Tye, C. E., Rattray, K. R., Warner, K. J., Gordon, J. A., Sodek, J., Hunter, G. K., and Goldberg, H. A., *J. Biol. Chem.* **278**, 7949–7955 (2003).
[10] Thurner, P. J., Erickson, B., Jungmann, R., Schriock, Z., Weaver, J. C., Fantner, G. E., Schitter, G., Morse, D. E., and Hansma, P. K., *Eng. Fract. Mech.* **74**, 1928–1941 (2007).
[11] Kindt, J. H., Thurner, P. J., Lauer, M. E., Bosma, B. L., Schitter, G., Fantner, G. E., Izumi, M., Weaver, J. C., Morse, D. E., and Hansma, P. K., *Nanotechnology* **18**, 135102-135108 (2007).
[12] Fantner, G. E., Hassenkam, T., Kindt, J. H., Weaver, J. C., Birkedal, H., Pechenik, L., Cutroni, J. A., Cidade, G. A. G., Stucky, G. D., Morse, D. E., and Hansma, P. K., *Nat. Mater.* **4**, 612–616 (2005).
[13] Thompson, J. B., Kindt, J. H., Drake, B., Hansma, H. G., Morse, D. E., and Hansma, P. K., *Nature* **414**, 773–776 (2001).
[14] Fantner, G. E., Adams, J., Turner, P., Thurner, P. J., Fisher, L. W., and Hansma, P. K., *Nano. Lett.* **7**, 2491–2498 (2007).
[15] Gupta, H. S., Fratzl, P., Kerschnitzki, M., Benecke, G., Wagermaier, W., and Kirchner, H. O., *J. R. Soc. Interface.* **4**, 277–282 (2007).
[16] Thurner, P. J., Wiley Interdisciplinary Reviews: Nanomedicine, in press.
[17] Ogbureke, K. U. and Fisher, L. W., *J. Dent. Res.* **83**, 664–670 (2004).
[18] Turner, C. H., *Osteoporos. Int.* **13**, 97–104 (2002).
[19] Bay, B. K., *J. Orthop. Res.* **13**, 258–267 (1995).

[20] Suzuki, K., Horiba, I., and Sugie, N., *Comput. Vis. Image Und.* **89**, 1–23 (2003).
[21] Nalla, R. K., Kinney, J. H., and Ritchie, R. O., *Nat. Mater.* **2**, 164–168 (2003).
[22] Fantner, G. E., Rabinovych, O., Schitter, G., Thurner, P., Kindt, J. H., Finch, M. M., Weaver, J. C., Golde, L. S., Morse, D. E., Lipman, E. A., Rangelow, I. W., and Hansma, P. K., *Compos. Sci. Technol.* **66**, 1205–1211 (2006).
[23] Tang, S. Y., Zeenath, U., and Vashishth, D., *Bone* **40**, 1144–1151 (2007).
[24] Nanci, A., *J. Struct. Biol.* **126**, 256–269 (1999).
[25] McKee, M. D., Addison, W. N., and Kaartinen, M. T., *Cells Tissues Organs* **181**, 176–188 (2005).
[26] Adams, J., Fantner, G. E., Fisher, L. W., and Hansma, P. K., *Nanotechnology* **19**, 384008 (2008).
[27] Zappone, B., Thurner, P. J., Adams, J., Fantner, G. E., and Hansma, P. K., *Biophys. J.* **95**, 2939–2950 (2008).
[28] Lin, Q., Gourdon, D., Sun, C., Holten-Andersen, N., Anderson, T. H., Waite, J. H., and Israelachvili, J. N., *Proc Natl. Acad. Sci. USA* **104**, 3782–3786 (2007).
[29] Gupta, H. S., and Zioupos, P., *Med. Eng. Phys.* **30**, 1209–1226 (2008).
[30] Peterlik, H., Roschger, P., Klaushofer, K., and Fratzl, P., *Nat. Mater.* **5**, 52–55 (2006).
[31] Koester, K. J., Ager, J. W., III, and Ritchie, R. O., *Nat. Mater.* **7**, 672–677 (2008).
[32] McKee, M. D., Farach-Carson, M. C., Butler, W. T., Hauschka, P. V., and Nanci, A., *J. Bone Miner. Res.* **8**, 485–496 (1993).
[33] McKee, M. D. and Nanci, A., *Microsc. Res. Tech.* **31**, 44–62 (1995).
[34] Goldsmith, H. L., Labrosse, J. M., McIntosh, F. A., Maenpaa, P. H., Kaartinen, M. T., and McKee, M. D., *Ann. Biomed. Eng.* **30**, 840–850 (2002).
[35] Hodgskinson, R. and Currey, J. D., *J. Mater. Sci.-Mater. M.* **3**, 377–381 (1992).